

Chapter 1

Introduction

The phenomena associated with the radiation interaction in matter are commonly understood to include a wide variety of physical effects. Moreover, the nature of interactions in matter depends on the incoming type of radiation and energy.

Furthermore, the incoming radiation also generates permanent or temporary damage. In most cases, detectors are not prevented from operating normally, but, in presence of large irradiations and/or as a result of large accumulated fluences, radiation effects may degrade devices performance. The second edition of this book is augmented by new chapters and additional sections have been added to some of the other chapters. Among these are treated radiation environments and basic mechanisms resulting in temporary and/or permanent radiation damages in devices, in particular those based on silicon semiconductor.

Historically, the first nuclear particle detectors (like those based on X -rays films) were very simple. In the course of time, the detectors have evolved toward higher specificity and at the same time toward more complexity. In addition, complex systems of detectors leading to large experimental apparatus often consist of several sub-detectors and require sophisticated methods of reconstruction and analysis of data to decrease the experimental errors. Therefore, both detectors and detection methods are fields of development and investigation.

In each application field, the detector configuration has to be designed to respond to the collision geometry, i.e., the experimental apparatus has to be capable to process the particles emerging from the interaction or production volume. For instance, for medical applications, the detection system needs to be adapted to the part of the patient's body under examination. In most cases, the large amount of data to analyze, their variety and often the large energy range to be covered can only be handled by the construction of detectors composed of many sub-detectors assigned to dedicated tasks. For example, in high energy physics experiments, collisions between two particles beams (*collider type of collision*) or by a beam hitting a fixed target (*fixed target type of collision*) produce a variety of particles, most of the time with very complicated configurations of events. Space-based experiments are another example of application where detector development is needed. These experiments aim at the study of astrophysics, gamma rays astronomy and cosmic rays,

interactions of cosmic rays with the space matter or with the Earth atmosphere or the detection of Galactic and extra-Galactic photons. The achievement of such vast research programs requires very reliable apparatus.

In this chapter (Chapter 1), an overview of the types of interactions in matter and the physical meaning of interaction cross section are presented. These interactions and their properties will be extensively discussed in the two following chapters (Chapters 2 and 3) from the phenomenological point of view: these features constitute fundamental principles for designing detection systems. In addition, the basic equations and relations of relativistic kinematics will be introduced. Finally, an overview of detection methods and detecting media will be given.

Radiation environments and processes resulting in displacement damage are addressed in Chapter 4.

In the following chapters, i) the scintillation processes and scintillating media (Chapter 5), ii) the *electron-hole* carriers formation, charge transport and damage effects in semiconductors employed as radiation detectors (Chapter 6), iii) radiation effects in silicon devices (Chapter 7), and iv) the signal generation in ionization chambers (Chapter 8) will be dealt with. The principles of particle energy determination for both electromagnetic and hadronic particles are discussed in Chapter 9. In Chapter 10, droplet detectors, their response to neutrons and α -particles, and, in addition, their usage for a search of cold dark matter are treated. In Chapter 11, detector applications for Medical Physics are considered.

A collection of *General Properties and Constants* is included in Appendices A.1–A.8. Elements of *Mathematics and Statistics* for detection systems are summarized in Appendices B.1–B.2.

Finally, excellent books, complementary to the current *Second Edition* (for the first edition see [Leroy and Rancoita (2004)]), are available on the topics of radiation interactions in matter and techniques in particle detection and measurements: for instance, without being comprehensive, the more recent are [Fernow (1986); Gilmore (1992); Leo (1994); Kleinknecht (1998); Knoll (1999); Green (2000); Wigmans (2000); Grupen and Shwartz (2008); PDB (2008)].

1.1 Radiation and Particle Interactions

Radiation is detected by its interaction in matter. Every detection system has the same structure: it starts with the interaction of the radiation with the detection medium; the result of the interaction is transformed into signals, which are readout and usually recorded. The interaction processes depend on both the type and energy of the incoming particles* (or photons). The energy ranges encountered also vary by

*An incoming particle is sometimes referred to as primary, while particles (or photons) produced or emitted in the interaction are sometimes referred to as secondary.

orders of magnitude. For example, the electromagnetic spectrum[†] (photons) covers many decades of frequencies. The situation is similar for charged particles. Their energy ranges from fractions of eV to 10^{20} eV, in the case of ultra-high energy cosmic rays. The detecting media to be used in a particular application have to be carefully selected as function of particle type and energy.

Instruments for radiation detection evolve as new technologies become available and, as a consequence, more and more sophisticated devices are made available to users, nowadays. For instance, complex, large and advanced instrumentation can be found in usage for applications ranging from nuclear medicine and health physics to experimental high energy particle and space physics.

In practice, books on instrumentation have to be oriented to application fields. Nevertheless, in order to understand the principle of operation of radiation detectors, a deep knowledge of the interaction of radiation with matter is required. Physical phenomena allowing detection often involve soft electrons or photons, or atomic and molecular excitations. This is the case even for energetic and very energetic incoming charged particles. Furthermore, except for the case of total absorption of the incoming particle like in high-energy physics calorimetry, the particle is assumed to lose only a small fraction of its energy inside the detecting medium.

The loss of energy by a charged particle is caused by the interaction of the electric field associated with the moving charge and the one generated by the electronic (and, in few cases, nuclear) structure of detecting media. This process is referred to as *energy-loss process* and allows the dissipation of energy inside the detecting medium itself.

For sufficiently extended absorbers, high-energy hadronic particles (see Sect. 1.2) deposit their energy through a series of strong interactions with nuclei or nuclear constituents of the detector absorbing medium. The emerging particles will lose their energy by subsequent strong interactions but mostly by energy-loss processes. Thus, a cascade of particles is generated and their energies are fully absorbed in the detecting medium. Similarly, electromagnetic cascades are generated by primary electrons, positrons and photons whose energy is degraded by electromagnetic interactions and energy-loss processes.

The fundamental mechanism, on which radiation detectors are based, is the dissipation of a fraction^{‡‡} of the incoming radiation-energy inside the detecting material. The transferred energy is distributed among excited states, which are capable of generating *carriers*, for instance, electrons-holes in semiconductors, ion pairs in gaseous devices, photons in scintillating media, etc.. These *carriers* are processed by appropriate readout elements, for instance, front-end electronics for semiconductor detectors and for gaseous devices, or photomultipliers for scintillating materials,

[†]The electromagnetic spectrum is subdivided into frequency regions, i.e., radiowaves, microwaves, infrared radiation, visible radiation, violet and ultraviolet radiation, X-rays and γ -rays.

^{‡‡}As mentioned above, in some type of large detectors the whole amount of energy is deposited.

etc.. Hence, the required radiation information (such as momentum, energy, velocity) can be obtained. For example, in gas based detectors, the energy dissipation process results in creating *ion pairs* (i.e., electrons and positive ions) which are separated and move under the influence of an applied external electric field. Typically about 30 eV are required to create an ion pair. However, due to the limited number of ion pairs generated in a low density medium like a gas, a multiplication is usually needed in order to have enough carriers to induce a charge signal in the readout electronics. In semiconductor detectors, the medium is denser and an *electron-hole pair* requires about 3.6 eV to be generated; usually, no multiplication is needed inside these devices. In scintillating materials, whose densities are typically about half of semiconductor densities, the energy dissipation process results in emitting photons (about an order of 100 eV are needed to emit a photon), a fraction of which can be conveyed onto the photodiode of a photomultiplier where, in turn, *photoelectrons* are emitted and subsequently multiplied.

It is worthwhile to mention that these topics are based on both progresses in understanding of physical phenomena and discoveries of physical effects. These advancements have been recognized by a number of Nobel Prizes, e.g., like those awarded to W.C. Röntgen (1901), H. Lorentz and P. Zeeman (1902), J.J. Thomson (1906), A.A. Michelson (1907), J.D. van der Waals (1910), M. von Laue (1914), W.H. Bragg and W.L. Bragg (1915), C.G. Barkla (1917), M. Planck (1918), A. Einstein (1921), N. Bohr (1922), R.A. Millikan (1923), M. Siegbahn (1924), J. Franck and G. Hertz (1925), A.H. Compton and C.T.R. Wilson (1927), L. de Broglie (1929), E. Fermi (1939), P.M.S. Blackett (1948), C.F. Powell (1950), W.B. Shockley, J. Bardeen and W.H. Brattain (1956), P.A. Čerenkov, I. Frank and I.Y. Tamm (1958), D.A. Glaser (1960), L.D. Landau (1962), L.W. Alvarez (1968) and G. Charpak (1992).

1.2 Particles and Types of Interaction

Nowadays, it is usual to omit the term *elementary* while referring to the so-called *elementary particles* in fields like particle and nuclear physics. In the first half of the past century, only a few particles^{††} were already discovered. At present, we know that these particles are final products from the interactions and decays of a very large number of particle states. This multitude of particles is proven to derive from i) a few fundamental constituent *fermions* of *spin* $\frac{1}{2}$, i.e., the *quarks* with fractional electric charges ($+\frac{2}{3}e$ and $-\frac{1}{3}e$, where e is the electron charge) and ii) the *leptons* (like the electron and its corresponding neutrino) with integral electric charge or neutral. For instance, neutrons and protons are built from a set of three quarks. These constituents interact by exchanging *spin* 1 *bosons*, which mediate three types of fundamental interactions: strong, electromagnetic and weak

^{††}Protons, neutrons, electrons, neutrinos and photons were among the particles already discovered.

interactions. A fourth interaction, gravitation, is mediated by a *spin 2 boson* (*graviton*). The *photon* mediates the electromagnetic interaction, W^\pm and Z the weak interaction, and the *gluon* the strong interaction.

Particles interacting via the *strong interaction* are known as *hadrons*. There are two main classes of hadrons: the *baryons*, with half-integral spin values, and the *mesons*, with integral spin values. For example, protons and neutrons are baryons, while pions are mesons. Protons and neutrons are constituents of nuclei and often referred to as *nucleons*. The strong interaction also provides the necessary binding forces to hold together nucleons inside the nucleus. Most of hadrons are unstable and are called *hadronic resonances*.

The *electromagnetic interaction* is usually responsible for most of non-nuclear interactions in physics beyond the *gravitational attraction*, and generates bound states in atoms and molecules. The *Quantum Electrodynamics Theory* (QED), one of the most successful theory in physics, allows extremely precise calculations of electromagnetic interactions of particles. *Weak interactions* are, for instance, responsible for processes like radioactive β -decays in nuclear physics. The gravitational force is the interaction involving massive bodies at very large distances. However, the gravitational force has negligible effect in particle–particle interaction at short distances.

The relative strengths of interactions at distances of $\simeq 10^{-18}$ cm are (see [Fernow (1986)] and references therein):

- strong interaction: 1
- electromagnetic interaction: $\approx 10^{-2}$
- weak interaction: $\approx 10^{-5}$
- gravitational interaction: $\approx 10^{-39}$

There is solid evidence that part of, if not all, the interactions are *unified*, i.e., are different aspects or manifestations of one single interaction. For instance, the electromagnetic and weak interactions have been unified in the *electroweak theory*, whose prediction of the existence of massive *gauge bosons*, W^\pm and Z , has been experimentally verified.

Another remarkable feature of nature is the existence of *antimatter*. For every particle (fermion or boson), there exists an antiparticle, which has the same mass and spin, but opposite values of electric charge and magnetic momentum. An example of antiparticle is the positron, which is the antiparticle of the electron.

It is customary (see for instance [Fernow (1986); Perkins (1986)] and Section 38 of [PDB (2008)]) to measure energies in *Mega* or *Giga* electron Volt (MeV or GeV) and to use conversion factors in such a way the *speed of light* c and the *reduced Planck constant*^{||} \hbar are set to 1 to simplify relativistic calculations.

^{||}The reduced Planck constant (also known as *Dirac constant*) \hbar is given by

$$\hbar \equiv \frac{h}{2\pi},$$

Nevertheless, in the present book, we will use the momenta in units of MeV/c or in GeV/c and the masses in units of MeV/c^2 or GeV/c^2 , except when otherwise explicitly indicated.

1.2.1 Quarks and Leptons

At present, experimental data support the picture in which the matter is built from two basic types of fermions, i.e., quarks and leptons. As mentioned before, quarks carry fractional electric charges ($+\frac{2}{3}e$ and $-\frac{1}{3}e$). Antiquarks carry opposite electric charges. There are different types of quarks distinguished by their *flavor*, i.e., u , d , s , c , b and t quarks. Their masses range from $\simeq 5 \text{ MeV}/c^2$ for the lightest quark (u) to $\approx 171.2 \text{ GeV}/c^2$ for the heaviest quark* (t). Baryons are built from three quarks, while mesons from quark-antiquark pairs. Ordinary matter is usually constituted of baryonic particles, like protons (stable) and neutrons (unstable). Mesons are unstable.

Leptons carry integral electric charges. Three types of negatively charged leptons are known: the electron (e), the muon (μ) and the tau (τ), whose masses are 0.511, 105.7 and 1777 MeV/c^2 , respectively. Their antiparticles are positively charged. Associated with negative leptons are neutrinos, which are neutral leptons: ν_e (with mass $< 2.2 \text{ eV}$), ν_μ (with mass $< 170 \text{ keV}$) and ν_τ (with mass $< 18.2 \text{ MeV}$). Neutrinos are longitudinally polarized with helicity $-\frac{1}{2}$ with regard to the direction of motion (they are *left handed*), while their correspondent antiparticles are *right handed* with helicity $+\frac{1}{2}$. The recent observation of neutrino oscillations implies that the neutrino has non-zero mass. This phenomenon, predicted by Pontecorvo whereby a neutrino created with a specific lepton flavor (ν_e, ν_μ, ν_τ) can later be observed to have a different flavor, is beyond the Standard Model of particle physics. At present, the experiments are only sensitive to the difference in the squares of the masses of neutrinos. These differences are known to be very small, i.e., $\lesssim 0.05 \text{ eV}/c^2$.

Charged leptons undergo both electromagnetic and weak interactions, while neutrinos only undergo weak interactions. Quarks can interact via electromagnetic, weak and strong interactions.

1.3 Relativistic Kinematics

In this section, we will recall a few basic formulae of relativistic kinematics. In addition, we will discuss the relativistic kinematics of the two-body collision process and, also, the invariant mass of a many-particle system.

In relativistic mechanics, the *momentum* \vec{p} of a material point of mass m_r and

where $h = 6.6260693 \times 10^{-34} \text{ J s}$ is the Planck constant (Appendix A.2).

*This is the value reported by the particle data group (e.g., see [PDB (2008)] and the web site: <http://pdg.lbl.gov>).

velocity \vec{v} is

$$\begin{aligned}\vec{p} &= m_r \vec{v} \\ &= m_r \vec{\beta} c,\end{aligned}\tag{1.1}$$

where

$$\vec{\beta} = \frac{\vec{v}}{c},\tag{1.2}$$

is the ratio between the material-point velocity and the speed of light c . The mass m_r is also referred to as the *relativistic mass* and is related to the *rest mass*, m_0 , by the so-called *Lorentz factor* γ :

$$m_r = \gamma m_0,\tag{1.3}$$

where

$$\gamma = \frac{1}{\sqrt{1 - \beta^2}}\tag{1.4}$$

and, conversely,

$$\beta = \frac{\sqrt{\gamma^2 - 1}}{\gamma}.\tag{1.5}$$

Thus, using Eq. (1.3), we can rewrite Eq. (1.1) as

$$\vec{p} = \vec{\beta} \gamma m_0 c\tag{1.6}$$

and consequently

$$\vec{\beta} \gamma = \frac{\vec{p}}{m_0 c}.\tag{1.7}$$

For the *total energy*, E , both the rest mass and the momentum have to be taken into account:

$$E = \sqrt{m_0^2 c^4 + p^2 c^2},\tag{1.8}$$

or, equivalently from Eqs. (1.2–1.4)

$$E = \sqrt{m_0^2 c^4 + m_r^2 \beta^2 c^4}\tag{1.9}$$

$$\begin{aligned}&= \sqrt{m_0^2 c^4 + (\gamma m_0)^2 \beta^2 c^4} \\ &= m_0 c^2 \sqrt{1 + \beta^2 \gamma^2} \\ &= \gamma m_0 c^2\end{aligned}\tag{1.10}$$

$$= m_r c^2.\tag{1.11}$$

The *kinetic energy* is given by

$$E_k = E - m_0 c^2\tag{1.12}$$

and using Eq. (1.10) one finds:

$$E_k = m_0 (\gamma - 1) c^2,\tag{1.13}$$

or, equivalently, using Eq. (1.4)

$$E_k = m_0 c^2 \left(\frac{1}{\sqrt{1 - \beta^2}} - 1 \right). \quad (1.14)$$

Furthermore, from Eqs. (1.8, 1.12), one can also express the momentum (p) as:

$$\begin{aligned} m_0^2 c^4 + p^2 c^2 &= (E_k + m_0 c^2)^2 \\ m_0^2 c^4 + p^2 c^2 &= E_k^2 + 2m_0 c^2 E_k + m_0^2 c^4, \end{aligned}$$

from which one obtains

$$p = \frac{\sqrt{E_k (E_k + 2m_0 c^2)}}{c} \quad (1.15)$$

Let us indicate with \mathcal{E} the quantity determined by the ratio

$$\mathcal{E} = \frac{E_k}{m_0 c^2}.$$

From Eqs. (1.10, 1.12), we have

$$\gamma = \mathcal{E} + 1; \quad (1.16)$$

thus, Eq. (1.5) can be rewritten as

$$\beta = \frac{\sqrt{\mathcal{E}(\mathcal{E} + 2)}}{\mathcal{E} + 1}, \quad (1.17)$$

and, finally, we get

$$\beta\gamma = \sqrt{\mathcal{E}(\mathcal{E} + 2)}. \quad (1.18)$$

The energy and the momentum of a particle in a second reference system, whose constant velocity is $-\vec{\beta}_0 c$ with respect to the original system, are obtained by the so-called *Lorentz transformations* (see for instance [Hagedorn (1964)]):

$$\vec{p} = \vec{p}' + \vec{\beta}_0 \gamma \left(\frac{\gamma}{\gamma + 1} \vec{\beta}_0 \cdot \vec{p}' + \frac{E'}{c} \right), \quad (1.19)$$

$$\frac{E}{c} = \gamma \left(\frac{E'}{c} + \vec{\beta}_0 \cdot \vec{p}' \right), \quad (1.20)$$

where E' and \vec{p}' are the energy and the momentum in the original reference system. Furthermore, under Lorentz transformations, a time interval τ elapsed in a coordinate system, where the particle is at rest, is dilated by the Lorentz factor in a coordinate system moving with a velocity $-\beta c$ with respect to the particle (namely in the system in which the particle moves with a speed βc):

$$t = \gamma\tau. \quad (1.21)$$

For example, in its rest frame, a charged pion with a rest mass $\approx 139.57 \text{ MeV}/c^2$ has a mean-life of $\approx 2.6 \times 10^{-8} \text{ s}$. From Eq. (1.21), at 10 GeV in the laboratory frame (i.e., $\gamma \approx 72$ and $\beta \approx 1$), it becomes $t \approx 72 \times 2.6 \times 10^{-8} \approx 1.87 \times 10^{-6} \text{ s}$. Before decaying, the pion path is $l = ct \approx 562 \text{ m}$.

1.3.1 The Two-Body Scattering

Radiation processes, like the ones resulting in energy losses by collision, take place in matter and can be considered (see following chapters) as two-body scatterings in which the target particle is almost at rest. In this section, we will study the kinematics of these processes and, in particular, derive equations regarding the maximum energy transfer.

Let us consider an incident particle [e.g., a proton (p), pion (π), kaon (K), etc.] of mass m and momentum \vec{p} , and a target particle of mass m_e [Rossi (1964)] at rest. For collision energy-loss processes, the target particle in matter is usually an atomic electron (see Fig. 1.1). After the interaction, two scattered particles emerge: the former with mass m and momentum \vec{p}'' and the latter with mass m_e and momentum \vec{p}' . The latter one has the direction of motion (i.e., the direction of the three-vector \vec{p}') forming an angle θ with the incoming particle direction. θ is the angle at which the target particle is *scattered*. The kinetic energy [see Eq. (1.12)] of the scattered particle is related to its momentum by

$$E_k + m_e c^2 = \sqrt{p'^2 c^2 + m_e^2 c^4}, \quad (1.22)$$

from which we get

$$p'^2 = \frac{(E_k + m_e c^2)^2 - m_e^2 c^4}{c^2}. \quad (1.23)$$

The total energy before and after scattering is conserved. Thus, we have

$$\sqrt{p^2 c^2 + m^2 c^4} + m_e c^2 = \sqrt{p''^2 c^2 + m^2 c^4} + E_k + m_e c^2$$

and, consequently,

$$\sqrt{p''^2 c^2 + m^2 c^4} = \sqrt{p^2 c^2 + m^2 c^4} - E_k, \quad (1.24)$$

while from momentum conservation:

$$\vec{p}'' = \vec{p} - \vec{p}' \quad \implies \quad p''^2 = p^2 + p'^2 - 2pp' \cos \theta. \quad (1.25)$$

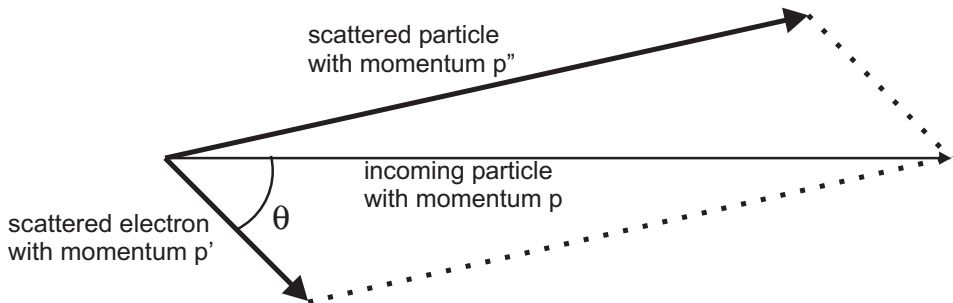


Fig. 1.1 Incident particle of mass m and momentum \vec{p} emerges with momentum $p'' = |\vec{p}''|$, while the scattered electron emerges with momentum $p' = |\vec{p}'|$.

Equation (1.25) can be rewritten taking into account Eq. (1.23):

$$p''^2 = p^2 + \frac{(E_k + m_e c^2)^2 - m_e^2 c^4}{c^2} - 2p \cos \theta \sqrt{\frac{(E_k + m_e c^2)^2 - m_e^2 c^4}{c^2}},$$

which becomes, after substituting p'' obtained from Eq. (1.24) and squaring both sides of that equation,

$$E_k \sqrt{p^2 c^2 + m^2 c^4} = -E_k m_e c^2 + p c \cos \theta \sqrt{(E_k + m_e c^2)^2 - m_e^2 c^4},$$

from which we get

$$p c \cos \theta \sqrt{\frac{E_k^2 + 2E_k m_e c^2}{E_k^2}} = m_e c^2 + \sqrt{p^2 c^2 + m^2 c^4},$$

and, finally, by squaring both sides of the equation we can derive the expression for the kinetic energy E_k of the scattered target particle, i.e.,

$$E_k = \frac{2m_e c^4 p^2 \cos^2 \theta}{\left(m_e c^2 + \sqrt{p^2 c^2 + m^2 c^4}\right)^2 - p^2 c^2 \cos^2 \theta}. \quad (1.26)$$

The kinetic energy E_k of the recoiling target particle is the amount of transferred energy in the interaction. From Eq. (1.26), we note that the maximum energy transfer W_m is for $\theta = 0$, i.e., when a head-on collision occurs. For $\theta = 0$, Eq. (1.26) becomes:

$$W_m = \frac{p^2 c^2}{\frac{1}{2} m_e c^2 + \frac{1}{2} (m^2 / m_e) c^2 + \sqrt{p^2 c^2 + m^2 c^4}}. \quad (1.27)$$

From Eq. (1.10), the incoming particle energy E_i is given by

$$E_i = m \gamma c^2 = \sqrt{p^2 c^2 + m^2 c^4}.$$

We can rewrite Eq. (1.27) as:

$$W_m = 2m_e c^2 \beta^2 \gamma^2 \left[1 + \left(\frac{m_e}{m}\right)^2 + 2\gamma \frac{m_e}{m} \right]^{-1}. \quad (1.28)$$

Massive particles (e.g., proton[§], K, π etc.) are particles whose masses are much larger than the electron (or positron) mass m_e , i.e.,

$$m \gg m_e (\approx 0.511 \text{ MeV}/c^2).$$

For massive particles, at sufficiently high energies[‡], i.e., when the incoming momentum p is

$$p \gg \frac{m^2}{m_e} c,$$

[§]The rest mass of the proton is $\approx 938.27 \text{ MeV}/c^2$.

[‡]For instance, this condition is satisfied by an incoming π with momentum $\gg 36 \text{ GeV}/c$ or an incoming proton with momentum $\gg 1.7 \text{ TeV}/c$.

Eq. (1.27) becomes

$$W_m \approx pc \approx E_i.$$

In the extreme relativistic case, a massive particle can transfer all its energy to the target electron in a head-on collision, i.e., a proton can be stopped by interacting with an electron. At lower energies[†], i.e., when

$$p \ll \frac{m^2}{m_e}c,$$

the maximum energy transfer [see Eq. (1.27)] by particles with $m \gg m_e$ is approximated by

$$W_m \approx 2m_e c^2 \left(\frac{p}{mc} \right)^2$$

and, because $p = m\beta\gamma c$, we have:

$$W_m \approx 2m_e c^2 \frac{\beta^2}{1 - \beta^2} = 2m_e c^2 \beta^2 \gamma^2. \quad (1.29)$$

For instance, a proton of 10 GeV has a Lorentz factor $\gamma \approx 10$ and $\beta \approx 1$. Thus, its maximum energy transfer is $W_m \approx 100$ MeV.

1.3.2 The Invariant Mass

The four-momentum of a particle with rest mass[‡] m_0 is defined as

$$\tilde{q} = \left(\frac{E}{c}, \vec{p} \right).$$

The scalar product between two four-momenta \tilde{q} and \tilde{q}' is an invariant** quantity and is given by (e.g., Section 38 of [PDB (2008)])

$$\tilde{q} \cdot \tilde{q}' = \frac{E E'}{c^2} - \vec{p} \cdot \vec{p}'. \quad (1.30)$$

The *invariant mass* of a particle is related to the scalar product of its four-momentum by:

$$\begin{aligned} \tilde{q} \cdot \tilde{q} &= q^2 \\ &= \frac{E^2}{c^2} - \vec{p} \cdot \vec{p} \\ &= \frac{E^2}{c^2} - p^2 \\ &= m_0^2 c^2 \end{aligned}$$

[†]For instance, this condition is satisfied by an incoming π with momentum $\ll 36$ GeV/c or an incoming proton with momentum $\ll 1.7$ TeV/c.

[‡]The *rest mass* is the mass of a body that is isolated (free) and at rest relative to the observer.

**The *invariant mass* or *intrinsic mass* or *proper mass* or *just mass* is the mass of an object that is the same for all frames of reference.

and, finally,

$$m_0 = \sqrt{\frac{\tilde{q} \cdot \tilde{q}}{c^2}}. \quad (1.31)$$

The invariant mass of a single particle is its rest mass.

The invariant mass, M , of a set of particles is the energy available in their center-of-mass system. It is given by

$$M = \sqrt{\frac{\tilde{q}_s^2}{c^2}} = \sqrt{\frac{[\sum_i (E_i/c)]^2 - (\sum_i \vec{p}_i) \cdot (\sum_i \vec{p}_i)}{c^2}}, \quad (1.32)$$

where

$$\tilde{q}_s = \sum_i \tilde{q}_i$$

is the total four-momentum. Let us consider two particles with masses m_1 and m_2 and momenta \vec{p}_1 and \vec{p}_2 . From Eq. (1.32), we have that their invariant mass $M_{1,2}$ is:

$$\begin{aligned} M_{1,2} &= \frac{1}{c} \sqrt{\left(\frac{E_1 + E_2}{c}\right)^2 - p_1^2 - p_2^2 - 2p_1 p_2 \cos \theta} \\ &= \frac{1}{c} \sqrt{2 \frac{E_1 E_2}{c^2} + m_1^2 c^2 + m_2^2 c^2 - 2p_1 p_2 \cos \theta}, \end{aligned} \quad (1.33)$$

where θ is the angle between the three-vectors \vec{p}_1 and \vec{p}_2 . For example, let us take a proton of 100 GeV incident on a target proton at rest in a high-energy physics fixed target experiment. From Eq. (1.33), because $p_2 = 0$, $E_2 = m_2 c^2$, $m_1 = m_2 \approx 1 \text{ GeV}/c^2$, the available center-of-mass energy (i.e., the invariant mass) becomes

$$M_{1,2} \approx \sqrt{200 + 1 + 1} \approx 14.2 \text{ GeV}/c^2.$$

Furthermore, in the scattering between an incoming particle 1 and a target particle 2, we define the invariant quantity s as:

$$\begin{aligned} s &= (\tilde{q}_1 + \tilde{q}_2)^2 \\ &= m_1^2 c^2 + m_2^2 c^2 + 2 \frac{E_1 E_2}{c^2} - 2\vec{p}_1 \cdot \vec{p}_2. \end{aligned} \quad (1.34)$$

If the particle 1 (2) emerges as particle 3 (4), the invariant quantity s is also given by

$$s = (\tilde{q}_3 + \tilde{q}_4)^2.$$

From Eq. (1.33), s is the invariant mass square of the system 1,2 (3,4) times c^2 , i.e., the square of the total energy in the center-of-mass system divided by c^2 . For the same reaction, we define the invariant quantity t as the *square of four-momentum transfer*:

$$t = (\tilde{q}_1 - \tilde{q}_3)^2 = (\tilde{q}_2 - \tilde{q}_4)^2 \quad (1.35)$$

$$= m_1^2 c^2 + m_3^2 c^2 - 2 \frac{E_1 E_3}{c^2} + 2\vec{p}_1 \cdot \vec{p}_3. \quad (1.36)$$

Both s and t are called *Mandelstam variables*. There is a third Mandelstam variable

$$u = (\tilde{q}_1 - \tilde{q}_4)^2 = (\tilde{q}_3 - \tilde{q}_2)^2.$$

However, it is not independent of s and t , as

$$s + t + u = m_1^2 c^2 + m_2^2 c^2 + m_3^2 c^2 + m_4^2 c^2.$$

1.4 Cross Section and Differential Cross Section

The cross section, σ , for a physical process is derived from the reaction probability for the occurrence of such an interaction. More precisely, when a collimated particle beam impinges on a target (see Fig. 1.2), some particles are removed by the physical reactions, resulting in an attenuated beam. The physical reactions occurring between the beam and the target particles include for example elastic scattering and particle production. A net difference between the incoming and outgoing particles can be measured and the removal probability of beam particles can be determined.

The simplest way of representing such a reaction is to imagine the incoming beam made of a uniform distribution of particles and the target as made of a disk onto which a certain amount of beam particles interact. This way, particles impinging onto the disk surface interact, while particle outside this surface continue their trajectory unaffected. However, this naive point of view has to account for the finite dimensions of both projectiles and target. This disk does not coincide with the *geometrical cross section* presented by the target and depicted by

$$\sigma_g = \pi R_g^2$$

in Fig. 1.2, where R_g is the physical (i.e., geometrical) radius of the target. It means the *effective area* struck by incoming point-like particles. This effective area is the so-called *total reaction cross section* (σ_{total} in Fig. 1.2) and takes into account the different types of reactions (often referred to as *partial cross sections*) between the projectile and the target. In interactions among particles, or particles and nuclei, or particles and atoms, the cross section size is usually expressed in units of *barn* indicated by b (see Appendix A.1):

$$1 \text{ b} = 10^{-24} \text{ cm}^2 = 10^{-28} \text{ m}^2.$$

Let us have a monochromatic beam of F_0 particles, for which σ_{total} is the total atomic cross section for all interaction processes between incoming particles

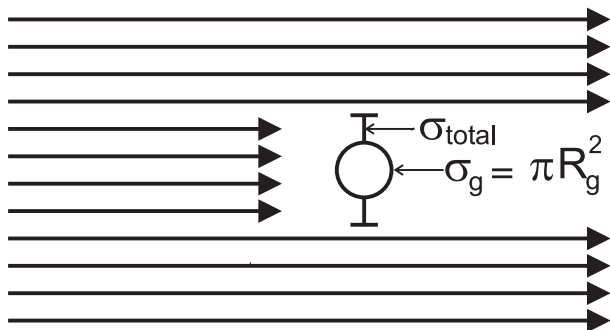


Fig. 1.2 Reaction and geometrical cross sections (see for instance [Marmier and Sheldon (1969)]).

and target atoms inside the absorber. In addition, we suppose that the overall absorber thickness is such that the probability of double particle interaction can be neglected. In the passage through a thickness dx' of the medium, the number of removed particles $-dF$ (the minus sign indicates that particles are removed from the beam) is proportional to the number of the beam particles F' at depth x' and to the number of target atoms per unit of volume, n_A , of the traversed material:

$$-dF = F' P_{\text{int}},$$

where $P_{\text{int}} = (\sigma_{\text{total}} dx') n_A$ is the probability of removing a particle in the thickness dx' . It has to be noted that n_A is the reciprocal of the atomic volume. We have:

$$\begin{aligned} -dF &= F' (\sigma_{\text{total}} dx') n_A \\ &= F' (\sigma_{\text{total}} n_A) dx' \\ &= \frac{F'}{\lambda_{\text{col}}} dx', \end{aligned}$$

where

$$\lambda_{\text{col}} = \frac{1}{n_A \sigma_{\text{total}}}. \quad (1.37)$$

The coefficient λ_{col} has the dimension of a length and is the so-called *collision length*, i.e., it is the *mean free path* between successive collisions. As a consequence, by traversing a thickness x of the absorber, we have:

$$\frac{dF}{F'} = -\frac{1}{\lambda_{\text{col}}} dx' \Rightarrow \int_{F_0}^F \frac{dF}{F'} = \int_0^x -\frac{dx'}{\lambda_{\text{col}}} \Rightarrow \ln \frac{F}{F_0} = -\frac{x}{\lambda_{\text{col}}},$$

and, finally,

$$F = F_0 \exp \left[-\left(\frac{x}{\lambda_{\text{col}}} \right) \right]. \quad (1.38)$$

Thus, there is an exponential decrease of the number of particles upon the passage in the absorbing medium.

The value of n_A , in units of cm^{-3} , is given by

$$n_A = \frac{N\rho}{A}, \quad (1.39)$$

where N is the *Avogadro constant* (see Appendix A.2), ρ is the absorber density, in g/cm^3 , and A is the *atomic weight* [also known as *relative atomic mass* (Sect. 1.4.1)]. The *number of electrons* per cm^3 , n , is given by

$$n = Zn_A = \frac{ZN\rho}{A}, \quad (1.40)$$

where Z is the *atomic number* (Sect. 3.1), i.e., the number of protons inside the nucleus of that atom. From Eqs. (1.37, 1.39), the expression for the collision length in cm can be rewritten as:

$$\lambda_{\text{col}} = \frac{A}{N\rho\sigma_{\text{total}}}, \quad (1.41)$$

where σ_{total} is in cm^2 .

An interaction, which results in the emission of a reaction product, can depend on parameters like the incoming energy or the emission angle. Therefore, we can introduce the so-called *differential cross section* to express the dependence of the emission probability on these parameters. For instance, the differential cross section per unit of solid angle $\frac{d\sigma}{d\Omega}$ gives, once multiplied by the solid angle element $d\Omega$, the incoming particle cross section to yield the reaction product into the element of solid angle $d\Omega$ lying at a mean angle θ with respect to the incident beam direction (the so-called *scattering angle*) and at a mean *azimuthal angle* ϕ . We have:

$$\sigma = \int_0^\Omega \frac{d\sigma}{d\Omega} d\Omega = \int_{\phi=0}^{2\pi} \int_{\theta=0}^{\pi} \frac{d\sigma}{d\Omega} \sin \theta d\theta d\phi,$$

where σ is the cross section for the reaction and $d\Omega = \sin \theta d\theta d\phi$.

1.4.1 Atomic Mass, Weight, Standard Weight and Atomic Mass Unit

The *atomic mass*** is the rest mass of an atom in its ground state. The commonly used unit is the unified atomic mass unit (indicated by the symbol u, see Appendix A.2). The *unified*†† *atomic mass unit*, as adopted by the International Union of Pure and Applied Chemistry (IUPAC) in 1966, is used to express masses of atomic particles and is defined to be exactly one twelfth of the mass of a ^{12}C atom in its ground state. The unified atomic mass unit replaced the *atomic mass unit* (chemical scale) and the *atomic mass unit* (physical scale), both having the symbol amu. The amu (physical scale) was one sixteenth of the mass of an atom of ^{16}O . The amu (chemical scale) was one sixteenth of the average mass of oxygen atoms as found in nature.

The *atomic weight* (also known as *relative atomic mass*†) of an element can be determined from the knowledge of the isotopic abundances and corresponding atomic masses of the nuclides (e.g., see [Tuli (2000); IUPAC (2006); NNDC (2008a)]) of that element as found in a particular environment: it is expressed by the ratio of the average, weighted by isotopic abundance, of atomic masses of all its isotopes to the unified atomic mass unit.

The *standard atomic weights* are the recommended values of relative atomic masses of the elements determined by their isotopic abundances in the surface and atmosphere of the Earth and are revised biennially by IUPAC. For instance, hydrogen has a standard atomic weight of 1.00794 [IUPAC (2006)] (see Appendix A.3 and references therein).

** As it is defined in the IUPAC Compendium of Chemical Terminology. The reader can see the web site: <http://www.iupac.org/goldbook/A00496.pdf>.

†† One unified atomic mass unit (u) is equal to $(1/N)$ gram, where N is the Avogadro constant.

‡ As it is defined in the IUPAC Compendium of Chemical Terminology. The reader can see the web site: <http://www.iupac.org/goldbook/R05258.pdf>.

It has to be noted that, in nuclear-physics, the symbol amu is the standard notation for particle masses expressed in relative atomic masses when, for example, ion kinetic-energies are given in MeV/amu or in GeV/amu. It is also of common usage, for instance in space physics, that these kinetic-energies (E_k) using Eq. (1.13) are expressed in MeV/nucleon or in GeV/nucleon (also termed *specific energy*, e.g., see Section 2.5.3 in [ICRUM (2005)]) as:

$$\frac{E_k}{M_A} = u c^2 (\gamma - 1),$$

where M_A is the mass number of the atom (Sect. 3.1). As noted in Section 2.5.3 of [ICRUM (2005)], in general no distinction is made between energy per nucleon and energy per atomic mass unit, because the small numerical difference[§] (e.g., see discussion in Sect. 3.1). Furthermore using Eq. (1.14), the specific energy of an ion at the Bohr velocity, $v_0 = c \alpha$ (see page 74 and Appendix A.2), is given by:

$$\left(\frac{E_k}{M_A} \right)_{v=v_0} = u c^2 \left(\frac{1}{\sqrt{1-\alpha^2}} - 1 \right) = 0.02489 \text{ MeV}.$$

1.5 Classical Elastic Coulomb Scattering Cross Section

Rutherford (1911) derived the classical differential cross section for the elastic Coulomb scattering of charged particles in connection with his proposal of atomic model. In this model, the atom consisted of a very small (i.e., almost point-like) nucleus surrounded by a more diffuse electron distribution. The mass and charge were supposed to be concentrated in the nucleus. This theory explained successfully experimental results^{††} from the scattering of α -particles upon gold target.

A complete derivation of the *Rutherford differential cross section* (also termed *Coulomb cross section* or *classical cross section*) can be found, for instance, in Section 2.1 of [Melissinos (1966)], in Section 3.5.7 of [Marmier and Sheldon (1969)] and in Section 2.2 of [Segre (1977)]. In the treatment, the incoming particle with charge ze^* , rest mass m and non-relativistic velocity[†] $v = \beta c$ scatters at an angle θ upon a target particle initially at rest with charge Ze and rest mass M under the action of a repulsive Coulomb force in the laboratory system. In the center-of-mass system (CoMS) for the reaction and assuming that the azimuthal distribution is

[§]The difference amounts to at most 0.25% for stable isotopes of all elements from lithium upward (Section 2.5.3 in [ICRUM (2005)]).

^{††}These results were obtained by Geiger and Marsden (1913).

* e is the electron charge.

[†]Under this assumption, we have $\gamma \simeq 1$, thus the kinetic energy and momentum of the incoming particle are $E_k \simeq mv^2/2$ and $p \simeq mv = m\beta c$, respectively.

isotropic, the differential cross section for scattering into a solid angle**

$$\begin{aligned} d\Omega' &= \int_0^{2\pi} d\varphi' d\cos\theta' \quad (\varphi' \text{ is the azimuthal angle}) \\ &= 2\pi \sin\theta' d\theta' \end{aligned}$$

is given in cgs esu units by:

$$\frac{d\sigma^{\text{Rut}}}{d\Omega'} = \left\{ \frac{zZe^2}{(mMv^2)/[2(m+M)]} \right\}^2 \left[\frac{1}{4\sin^2(\theta'/2)} \right]^2 \quad (1.42)$$

$$= \left\{ \frac{zZe^2}{(4ME_k)/(m+M)} \right\}^2 \frac{1}{\sin^4(\theta'/2)}, \quad (1.43)$$

where θ' is the scattering angle[‡] {see Equation (3.124) of [Marmier and Sheldon (1969)]}.

Furthermore, for $M \gg m$ the distinction between laboratory (i.e., the system in which the target particle is initially at rest) and center-of-mass system disappears and $\theta \approx \theta'$; thus, Eqs. (1.42, 1.43) reduce to *Rutherford's formula*

$$\frac{d\sigma^{\text{Rut}}}{d\Omega} \simeq \left(\frac{zZe^2}{2p\beta c} \right)^2 \frac{1}{\sin^4(\theta/2)} \quad (1.44)$$

$$= \left(\frac{zZe^2}{4E_k} \right)^2 \frac{1}{\sin^4(\theta/2)}$$

$$= \left(\frac{zZe^2}{2} \right)^2 \frac{1}{4E_k^2 \sin^4(\theta/2)}. \quad (1.45)$$

For E_k in MeV, Eq. (1.45) is re-expressed as

$$d\sigma^{\text{Rut}} \simeq 0.12951 \times 10^{-26} \times \left(\frac{zZ}{E_k} \right)^2 \frac{1}{\sin^4(\theta/2)} d\Omega \text{ [cm}^2/\text{nucleus]}. \quad (1.46)$$

Rutherford's formula is non-relativistic and is valid for a fixed scattering center. In addition, it does not account for nuclear forces. Nevertheless, in practice it can be considered an appropriate approximation for describing particle scattering, when this occurs at a distance to the target particle larger than its nuclear radius [see Eq. (3.12)]. It has to be noted that, for a small angle scattering, Eq. (1.44) becomes

$$\frac{d\sigma^{\text{Rut}}}{d\Omega} \simeq \left(\frac{2zZe^2}{p\beta c} \right)^2 \frac{1}{\theta^4}. \quad (1.47)$$

This equation is also valid at relativistic velocities (e.g., see discussion in Section 2.2 of [Segre (1977)]). Rutherford's formula can also be obtained using, for instance, the *Born approximation** in a quantum mechanical approach (e.g., see Section 2.2 and Appendix A of [Segre (1977)]).

**This corresponds to an angular aperture between θ' and $\theta' + d\theta'$.

‡For the scattering angle we have $0^\circ < \theta' < 180^\circ$.

*In quantum mechanical potential scattering, the scattered wave may be obtained by the so-called Born expansion. The Born approximation is the first term of the Born expansion (e.g., see Sections 3-1-3-2a of [Roman (1965)] and Section 7.2 of [Sakurai (1994)]).

Let us now derive the expression for the differential cross section with respect to the transferred energy in the scattering. We can compute the quantity t , i.e., the square of the four momentum transfer^{††}, in i) the laboratory system where the target particle, initially at rest, recoils with a kinetic energy T equal to the amount of energy transferred in the reaction and ii) the CoMS where the incoming particle with momentum p_{cm} is scattered[‡] at an angle θ' . Because the square of the four momentum transfer is an invariant quantity, from Eqs. (1.35, 1.36) we have

$$\begin{aligned} 2M^2c^2 - \frac{2Mc^2(Mc^2 + T)}{c^2} &= 2mc^2 - \frac{2(p_{\text{cm}}^2c^2 + m^2c^4)}{c^2} + 2p_{\text{cm}}^2 \cos \theta' \\ 2M^2c^4 - 2Mc^2(Mc^2 + T) &= 2(p_{\text{cm}}^2c^2 \cos \theta' + mc^4) - 2(p_{\text{cm}}^2c^2 + m^2c^4) \\ -2MT &= -2p_{\text{cm}}^2(1 - \cos \theta') \end{aligned}$$

and, consequently,

$$T = \frac{p_{\text{cm}}^2}{M} (1 - \cos \theta'). \quad (1.48)$$

The incoming particle momentum in the CoMS can be expressed in terms of incoming-particle laboratory momentum and rest mass of the particles (e.g., see Equation 38.6 of [PDB (2008)]):

$$p_{\text{cm}} = p \frac{M}{M_{\text{cm}}},$$

where M_{cm} is the reaction invariant-mass, which can be computed using Eq. (1.33); thus, we obtain

$$p_{\text{cm}} = p \frac{M}{\sqrt{m^2 + M^2 + 2M\sqrt{(p/c)^2 + m^2}}}. \quad (1.49)$$

The quantity $\cos \theta'$ can be rewritten as:

$$\begin{aligned} \cos \theta' &= \cos^2(\theta'/2) - \sin^2(\theta'/2) \\ &= 1 - 2 \sin^2(\theta'/2). \end{aligned} \quad (1.50)$$

Using Eqs. (1.49, 1.50), Eq. (1.48) becomes

$$\begin{aligned} T &= \left[\frac{p^2 M}{m^2 + M^2 + 2M\sqrt{(p/c)^2 + m^2}} \right] [2 \sin^2(\theta'/2)] \\ &= \frac{2p^2 M}{m^2 + M^2 + 2M\sqrt{(p/c)^2 + m^2}} \sin^2(\theta'/2). \end{aligned} \quad (1.51)$$

In a non-relativistic scattering for which $pc \ll mc^2$, Eq. (1.51) reduces to

$$\begin{aligned} T &\approx \frac{2p^2 M}{m^2 + M^2 + 2Mm} \sin^2(\theta'/2) \\ &= \frac{2p^2 M}{(m + M)^2} \sin^2(\theta'/2) \\ &= \frac{4mME_k}{(m + M)^2} \sin^2(\theta'/2) \end{aligned} \quad (1.52)$$

^{††}The reader can see page 12 and, also, discussion in Sect. 1.3.2.

[‡]In the CoMS, the scattering angle is the rotation angle of the particle momentum.

{e.g., see Equation (2-62) of [Ziegler, Biersack and Littmark (1985a)] or, equivalently, Equation (2-75) of [Ziegler, J.F. and M.D. and Biersack (2008a)]}. It has to be noted that the maximum energy transfer^{||} T_{\max} occurs for $\theta' = 180^\circ$, i.e., in case of a *head-on repulsive collision*, and is given by

$$T_{\max} = \frac{4mME_k}{(m+M)^2}; \quad (1.53)$$

thus, the recoil energy can be written as

$$T = T_{\max} \sin^2(\theta'/2). \quad (1.54)$$

Since [e.g., see Eq. (1.50)]

$$\begin{aligned} d\Omega' &= 2\pi \sin \theta' d\theta' \\ &= 2\pi d \cos \theta' \\ &= 4\pi d[-\sin^2(\theta'/2)], \end{aligned}$$

using Eq. (1.52) we can rewrite the Rutherford cross section [Eq. (1.43)] in terms of the recoil kinetic energy of the target particle (i.e., in terms of the energy transferred in the Coulomb interaction) as:

$$\begin{aligned} d\sigma^{\text{Rut}} &= \left\{ \frac{zZe^2}{(4ME_k)/(m+M)} \right\}^2 \frac{1}{\sin^4(\theta'/2)} d\Omega' \\ &= \left\{ \frac{zZe^2}{(4ME_k)/(m+M)} \right\}^2 \left[\frac{4mME_k}{T(m+M)^2} \right]^2 4\pi d[-\sin^2(\theta'/2)]. \end{aligned}$$

In the latter equation we can introduce Eq. (1.43), thus, we get:

$$\begin{aligned} d\sigma^{\text{Rut}} &= 4\pi \left[\frac{mzZe^2}{T(m+M)} \right]^2 \frac{(m+M)^2}{4mME_k} |d(-T)| \\ &= \pi \frac{m(zZe^2)^2}{ME_k} \frac{1}{T^2} dT, \end{aligned}$$

where the negative sign in the term $d(-T)$ indicates that the incoming particle loses energy as a result of the interaction[§]; this energy is absorbed via the target recoil. Finally, the differential cross section corresponding to a transferred energy between T and $T+dT$ (e.g., see Equation 7 of [Bakale, Sowada and Schmidt (1976)]) is given by

$$\begin{aligned} \frac{d\sigma^{\text{Rut}}}{dT} &= \pi \frac{m(zZe^2)^2}{ME_k} \frac{1}{T^2} \\ &= 2\pi \frac{(zZe^2)^2}{Mv^2} \frac{1}{T^2}. \end{aligned} \quad (1.55)$$

In Coulomb interactions, for instance those resulting in displacement damage for silicon devices (e.g., see discussions in Sects. 4.2.1.3 and 7.1.3), the average energy

^{||} T_{\max} can also be obtained using Eq. (1.27) for $\gamma = 1$.

[§]The Coulomb scattering of charged particles on atomic electrons is the dominant mechanism of *collision* (also termed *electronic energy-loss process* discussed, for instance, in Sect. 2.1.1.

transferred in the reaction determines the extension of the subsequent cascade development of atomic displacements. Assuming that the interaction is purely electrostatic and neglecting the screening effect* of nuclear Coulomb potentials, to a first approximation the average energy transferred $\langle T \rangle$ above a minimum energy threshold E_{\min} up the maximum energy-transfer can be obtained by means of Eq. (1.55) and it is expressed as:

$$\begin{aligned} \langle T \rangle &= \int_{E_{\min}}^{T^{\max}} \frac{d\sigma^{\text{Rut}}}{dT} T dT \bigg/ \left(\int_{E_{\min}}^{T^{\max}} \frac{d\sigma^{\text{Rut}}}{dT} dT \right) \\ &= \int_{E_{\min}}^{T^{\max}} \frac{1}{T} dT \bigg/ \left(\int_{E_{\min}}^{T^{\max}} \frac{1}{T^2} dT \right) \\ &= \frac{E_{\min} T^{\max}}{T^{\max} - E_{\min}} \ln \left(\frac{T^{\max}}{E_{\min}} \right). \end{aligned} \quad (1.56)$$

1.6 Detectors and Large Experimental Apparata

Radiation detectors use *detecting* (sometime referred to as *active*) *media* and *read-out* systems. The operation of any detecting device is based on specific effects of radiation interaction in matter. These effects are exploited in order to produce quantitative measurable signals in the readout system associated with the detection system itself.

The basic features of radiation detectors can be understood once fundamental processes of radiation interaction in matter are considered (see chapters on *Electromagnetic Interaction of Radiation in Matter* and on *Nuclear Interactions in Matter*). For instance, the collision energy-loss is the mechanism generating primary electrons (which in turn can generate secondary electrons) in gaseous detectors, or excited molecules (which decay emitting photons) in scintillating devices, or electron-hole pairs in semiconductors, etc.. The primary mechanism of transferring energy from an incoming charged particle to a medium has to enable the generation of secondary detectable particles, whose number or flux of energy has to be as much as possible linearly related to the incoming number of particles or incoming particle energy. Radiation detectors, or combinations of them, can provide a wide range of information as spatial locations, particle momentum, velocity, energy, etc..

For instance, in nuclear medicine, the image formation is based on the spatial reconstruction of the radiation emitted from a patient. The detecting system needs to be complex and consists of many sub-detectors in order to cover large emission area and provide a 3-dimensional reconstruction of the internal volume of the patient under investigation. In high-energy physics experiments, detectors are located downstream a fixed target or surrounding the collision point in colliding beams ma-

*The screening of the Coulomb potential cannot be neglected at low energy (e.g., see discussion in Sect. 4.2.1.3).

chines. In space experiments, sets of highly reliable detectors are located on board of satellites and recently on board of the International Space Station for photons and energetic cosmic rays detection. Particles created in high energy collisions or impinging on a space detector, pass through various types of detectors with dedicated tasks. Examples are:

- tracking, with capability of momentum analysis in *magnetic spectrometers*,
- electron and hadron separation,
- particle identification,
- energy determination,
- triggering,
- data acquisition,
- monitoring.

Each sub-detector has very specific characteristics and its functionality has to be optimized taking into account the features of other sub-detectors.

Particles passing through *tracking detectors* (or *trackers*) have their trajectories reconstructed by dedicated computer software codes. The accuracy of reconstructed trajectories depends on the spatial resolution of the tracker, which can be of a few μm 's for *semiconductor detectors* (see the chapter on *Solid State Detectors*), $\approx 100 \mu\text{m}$ for *drift chambers* and a few hundreds μm 's for *MultiWire Proportional Chambers* (MWPC). The two latter ones are gas based devices. The accuracy also depends on the multiple Coulomb scattering inside the tracker. In *magnetic spectrometers*, the particle momentum can be determined once the particle trajectory has been reconstructed.

As will be discussed in details in this book, electrons, photons and hadrons can create electromagnetic and hadronic showers in matter (see Sects. 2.4 and 3.3). The characteristics of the shower can be determined with calorimeters, as discussed in the chapter on *Principles of Particle Energy Determination*. These detectors can measure both the energy and the impact position of the incoming particle. In addition, the distribution of energy deposition along and perpendicularly to the incoming particle direction is used to discriminate among incoming electrons/photons and hadrons.

Other devices, such as the *Transition Radiation Detectors* (TRD), can provide signatures for discriminating electrons from hadrons at high energy. These devices are classified among the so-called *particle identification detectors*, like the *Čerenkov detectors*.

All the detectors or sub-detectors in an experiment or in a large, complex detection system must be carefully integrated. The design system does not need to exploit all the best sub-detector features. It only needs to make them suited to the purpose of the overall resulting apparatus. Fast outputs from sub-detectors or dedicated detectors provide *trigger signals*, which indicate that a particular type of *event* has occurred inside the apparatus. The trigger looks for spatial and/or

temporal correlation of detectors or sub-detector signals, which have been set in designing the apparatus. The trigger can also be based on threshold, such as energy threshold.

Calibration and on-line monitoring are tasks which have to be particularly investigated and implemented in large and complex apparatus. Data are usually collected via a *data acquisition system* (DAQ), which sends them or part of them to monitoring computer codes and the recording system.

Computers play a central role in processing data and afterwards in displaying processed data. Much of the software code used in the reconstruction of physical events is detector or apparatus dependent. Graphical routines for data display are by themselves an important field of continuous development and require more and more powerful processors.

1.6.1 *Trigger, Monitoring, Data Acquisition, Slow Control*

A trigger signal is an electronic signal which indicates the occurrence of an *event* which has to be processed and, possibly, collected by the data acquisition part of the apparatus. A well designed trigger avoids the data collection system to be swamped by similar but background events. This way, expected events together with a minimal amount of background events will be collected and processed. For instance, the trigger can be constructed to identify particles, to separate electrons from hadrons, to count the event multiplicity, etc.. For large apparatus, the trigger is organized with a few levels following a hierarchical sequence. Programmable devices are commonly employed such as look-up tables, hard-wired processors, microprocessors, emulators.

In recent years, the pipelined processing has been often adopted in order to avoid loss of information. It is typically employed for event recording and storage in high performance computing systems. There are different types of pipelines for storing signals coming from various parts of the apparatus. The pipeline can be both analog and digital.

Particularly interesting events, as well as events sampled on a statistical basis, can be passed to the on-line event display task. This latter task can be integrated inside the on-line monitoring and calibration tasks, which allow us to verify that the whole detector is properly functioning during the data collection. Within this framework, automatic processes search for anomalous behaviors of sub-detectors and send warning messages or try to readjust remote controlled sub-detector elements to restore the working condition. Sets of calibration constants are also collected in systematically updated databases and used in reconstruction procedures.

The term “data acquisition” includes the data collection from the whole apparatus, data storage on accessible media and subsequently to external software codes for reconstruction and display.

Complex detector systems usually require that sub-detector operations and re-

adjustments be carried out by dedicated remote software codes. Independently, if the event has to be considered or not as a background event, sub-detector operations are expected to be performed properly when some detector parameters are within predefined value ranges. These quantities are for instance high voltages and currents of sub-detectors, flow of gases (for gaseous detectors), temperature distribution, etc.. The slow control includes the recording, monitoring and control of all parameters which are expected to be within predefined ranges during data collection.

1.6.2 General Features of Particle Detectors and Detection Media

The spatial resolution depends on the detector type and, among detectors using similar media, on the type of readout system. The *resolution time* and the *dead time*[¶] also depend both on the detector type. Fast *drift chambers* have resolution times of $\simeq 2$ ns and dead times of $\simeq 100$ ns. Scintillator devices can reach resolution and dead times of about (100–150) ps and 10 ns, respectively. *Photographic emulsions* have spatial resolution of $\simeq 1 \mu\text{m}$. *Silicon strip*^{*} and *silicon pixel detectors* can achieve spatial resolutions of \simeq a few mm and $2 \mu\text{m}$ (and less), respectively.

The *photomultiplier* is a suitable vacuum tube designed as a source of primary electrons (*photoelectrons*) emitted by the photocathode and as a tool of electron amplification by secondary emission process. The amplification factor can be as large as 10^7 (for 12 stages). Photomultipliers are widely used in association with detection media in which photons are emitted, like scintillators and Čerenkov detectors. Photomultiplier operations can be limited, or even completely impaired, inside strong magnetic fields.

Organic scintillators are classified as organic crystals (i.e., anthracene, naphthalene, etc.), liquids^{||} or plastics^{**} depending on the type of the scintillating medium in usage and their densities are between $\simeq (1.03\text{--}1.25) \text{ g/cm}^3$. The scintillation mechanism is particularly noticeable in organic substances containing aromatic rings, for instance polystyrene, polyvinyltoluene and naphthalene. In liquid scintillator, molecules of toluene and xylene are typically included. About 3% of the deposited energy is re-emitted as optical photons. By far, the plastic scintillators are the most widely employed. Photon emission yields are approximately 100 eV of energy deposited inside the scintillating medium (see chapter on *Scintillating Media and*

[¶]The dead time is the time during which a detector is not capable of detecting a next coming particle.

^{*}One of the first examples of the usage of silicon strip and (in a second time also) microstrip detectors was for the active Si-target of the NA14 experiment at CERN-SPS [Rancoita and Seidman (1982); Barate et al. (1985)]; another was the microstrip detectors assembled as a silicon counter telescope for the target of the NA11 experiment [Rancoita and Seidman (1982); Belau, Klanner, Lutz, Neugebauer and Wylie (1983)].

^{||}In a liquid scintillator an organic crystal (solute) is dissolved in a solvent.

^{**}Plastic scintillators are similar in composition to liquids. Polystyrene and polyvinyl toluene are commonly used as base plastics to replace the solvent.

Scintillator Detectors). A *minimum ionizing particle** can generate up to 2×10^4 photons traversing ~ 1 cm of plastic scintillator. However, only a small fraction, typically less than 10%, of the generated photons arrive on the photomultiplier photocathode, whose *quantum efficiency*† does not exceed $\sim 30\%$ for the most favorable photon frequency. In addition, local ionizations much larger than those generated by minimum ionizing particles emit less light. Plastic scintillators are reliable and robust. With their high hydrogen content, they are particularly suited for neutron detection. However, their light yield degrades due to aging effects. For instance, aging can be enhanced by exposure to solvent vapors, irradiation and mechanical flexing. The radiation damage depends not only on the integrated dose, but on the dose rate, and environmental factors (like temperature and atmosphere) before and after the irradiation, as well as on material properties. Commonly used inorganic scintillators have larger densities, between $\simeq (3.67\text{--}8.28)$ g/cm³. They are very efficient for the detection of electrons and photons; they are employed when large densities and good energy resolution are required.

Detectors using a gas, or more likely a mixture of gases, have undergone a great deal of development since the first planar detector geometry: the MWPC (Multi-Wire Proportional Chamber), realized a few decades ago. This planar geometry has allowed one to exploit the cylindrical gas detector properties (see the chapter on *Ionization Chambers*) regarding both the small electron multiplication volume around the anode wire and the large drift volume available to positive ions at almost constant electric field towards the cathode. In the detector, ion pairs are generated in a gas layer, whose thickness is typically between a few cm's and a fraction of a cm. Anodes are regularly separated by less than 2 mm, but not much less than 1 mm, because there are practical difficulties of precisely stringing wires below 1 mm and in addition the mechanical tension, balancing the electrostatic force between wires, cannot exceed its critical value. This allows the achievement of spatial resolutions up to a few hundreds μm . These detectors need an individual readout channel per anode. Similar or even better spatial resolutions, with a small readout channel density, can be achieved with the so-called *drift chambers*. In these devices, the position of the passing particle is determined by the time difference between the passage of the particle and the arrival of electrons at the wire. Detectors (the so-called *time projection chamber*) with long drift distances perpendicularly to a multi-anode proportional plane provide three-dimensional information. Large volume chambers up to a few tens of m³ and several thousands of wires have been successfully operated in high energy physics experiments. The anode spacing limitation can be overcome by using lithographic technique, which have been able to produce a miniaturized version of a MWPC with thin aluminum strips engraved in an insulating support and an anode spacing reduced to (0.1–0.2) mm.

Silicon detectors are the most widely used semiconductor detectors. They are *p-n*

*The reader can see the definition at page 47.

†The quantum efficiency is the probability of emitting a photoelectron per impinging photon.

junction diodes operated in reverse bias (see chapter on *Solid State Detectors*). Their substrate is typically *n*-type high resistivity silicon with thickness between (300–500) μm . Full depletion voltages are usually between (50–150) V for 300 μm thick detectors, depending on their resistivity. The energy needed to be deposited inside the detector active volume to create an *electron–hole* (*e-h*) pair is about 3.6 eV. Electrons and holes are referred to as *carriers*. A minimum ionizing massive particle[‡] loses on average approximately 30 keV per 100 μm in a silicon detector,[§] i.e., it generates approximately 83 *e-h* pairs/ μm . The *transit time*, i.e., the time needed by carriers to drift towards the electrodes and, consequently, to induce electric signals on them, decreases as the reverse bias voltage necessary for full depletion increases. Typical transit times are ≤ 10 ns for electrons and ≤ 25 ns for holes in the case of a fully depleted 300 μm thick device. The transit time is mainly limited by the carrier mobility saturation for electric field larger than $\simeq 10^4$ V/cm. In the beginning of the 1960s, first demonstrations were made that silicon detectors operated at room temperature could be used for nuclear reaction studies and spectroscopy. Since then, a great deal of work and combined efforts have been carried out, making this type of detectors more and more reliable and easy to operate. Up to the beginning of the 1980s, these devices were expensive and with active areas not exceeding a fraction of 1 cm^2 . At that time (see for instance [Rancoita and Seidman (1982)]), the need to use them in high-energy physics experiments has resulted in developing large area *strip silicon detectors*, at relatively low cost. A further important step was the development of monolithic front-end electronics. Thus, a high density of readout channels (for instance one readout channel every 50 μm) could be achieved. Their usage as tracking devices has allowed the construction of complex detectors with some m^2 of overall active area. A subsequent development has achieved a three-dimensional readout by employing both the so-called *pixel silicon detectors* (Sect. 6.5) and the *double sided silicon detectors*.

As discussed in the chapter on *Principles of Particle Energy Determination* (see for instance [Leroy and Rancoita (2000)] and references therein) around mid-eighties, high energy sampling calorimeters using silicon detectors as active medium were developed for particle physics experiments. Very large active areas of silicon detectors have been realized for both high energy and space physics applications.

Silicon diodes can be used as photodiodes. Their quantum efficiencies are $> 70\%$ for photon wavelengths between ~ 600 nm and 1 μm . In practical applications, for instance in detecting photons from a scintillator, attention has to be paid to make sure that the detected signal due to photon conversion is larger than that due to the energy loss of particles traversing simultaneously the photodiode.

Both silicon detectors and photodiodes can work properly even in strong magnetic fields.

[‡]A massive particle is at the minimum of energy-loss for $\beta\gamma \approx 3$ (see page 47).

[§]Since fast δ -rays are not fully absorbed in thin absorbers, the average energy-loss per 100 μm can depend on the detector thickness, see Sect. 2.1.1.4.

Radiation damage can impair the silicon device performance. Nevertheless, if properly designed and associated with well suited front-end electronics, it can maintain its performance in large radiation fluence environments. Radiation damage causes the creation of *Frenkel pairs*, i.e., pairs consisting of a displaced atom from a lattice site and the corresponding vacancy in the previously occupied lattice site. This leads to i) a dose dependent increased leakage-current, ii) the creation of deep and shallow defects which can act as carrier trapping centers, iii) the build up of space charge able to change (i.e., to highly increase) the required reverse bias for achieving full depletion, etc.. In addition, there are surface damages resulting in an increase of the surface leakage current. In strip detectors, the inter-strip isolation is usually affected.

Particle identification detectors are designed to determine the particle rest mass m_0 once the measurement of particle momentum $p = m_0\beta\gamma c$ (see page 6) has been performed by other detectors. At low energy, e.g., for nuclear and particle physics applications, the particle velocity ($= \beta c$) can be measured by using the *time-of-flight* technique, i.e., by determining how much time it takes for the particle to pass through two subsequent detectors. For instance, time-of-flight systems using two plastic scintillators 1 m apart are able to provide a good particle mass identification for electrons, pions, kaons and protons up to particle momenta of $\approx (1.5-2)$ GeV/c for time resolutions of $\approx (120-150)$ ps.

Čerenkov detectors exploit the properties of the Čerenkov radiation (described in Sect. 2.2.2), which depends on the particle velocity. Threshold Čerenkov counters provide an information whether the particle is above or below the threshold velocity for emitting Čerenkov radiation in the radiator medium. Differential Čerenkov counters exploit the dependence on both the particle velocity and the emission angle of the emitted radiation. Finally *Ring Imaging Čerenkov Detectors* (RICH) exploit the properties of the Čerenkov radiation in geometries up to the full solid angle. These devices typically include more than one radiator medium.

Transition radiation (described in Sect. 2.2.3) is emitted when a charged particle crosses the boundaries of two media with different dielectric constants. Emitted photon energies depend both on the medium plasma frequency and on the *Lorentz factor* γ of the particle. In practice, the transition radiation becomes useful for particle detection when Lorentz factors are larger than 1000. The transition radiation devices are usually employed to provide electron/hadron separation in the energy range $0.5 \leq p \leq 100$ GeV/c, when soft *X-rays* radiated by electrons have energies of several keV's and can be detected inside wire chambers operated with gas mixtures containing xenon. A *Transition Radiation Detector* (TRD) is typically composed of several modules, each made of an *X-ray* detector and a radiator. The radiator is subdivided in order to have several hundred boundaries, because the photon probability emission is of $\simeq 1\%$ per boundary crossing. The TRD performance depends on its overall length.

The development of electromagnetic and hadronic showers is described in

Sects. 2.4 and 3.3, respectively. These showers differ largely both for their longitudinal (i.e., along the incoming particle direction) and transversal (i.e., on the plane perpendicular to the incoming particle direction) shapes. By exploiting these characteristics, the electron/hadron identification is achieved in calorimetry. *Calorimeters*, as discussed in the chapter on *Principles of Particle Energy Determination*, are devices in which the total incoming particle energy is deposited by a multiplicative process called the *cascading shower development*. In homogeneous calorimeters, the incoming particle releases its energy in a medium which is at the same time the *passive absorber* shower generator and the *active detection medium*. These calorimeters can achieve the best energy resolution and are typically employed for particles depositing their energy by electromagnetic cascades. Sampling calorimeters, mostly used for high energy electromagnetic and hadronic showers, consist in passive absorber layers interspaced with active detection media layers. This way, only a small fraction of the incoming particle energy, usually less than a few percents or even a fraction of percent, is deposited in the active part of the detection system. The *sampling fluctuations* are dominating the electromagnetic calorimeter energy resolution and are largely contributing to the overall hadronic calorimeter resolution. Because physical mechanisms by which energy is deposited in matter by electromagnetic and hadronic showers are different, care has to be given in hadronic calorimetry in equalizing the hadronic and the electromagnetic responses of the calorimeter, i.e., by achieving the so-called *compensation condition* (e.g., to achieve the ratio $e/\pi = 1$). In fact, contrary to electromagnetic cascades initiated by electrons and photons, cascades initiated by hadrons will proceed by generating both hadronic particles and particles showering via electromagnetic cascades, i.e., a hadronic shower will always contain some electromagnetic sub-cascades, due to the production in cascading of neutral particles (like π^0 , η , ...) decaying into photons. Electromagnetic sampling calorimeters typically have a response which is proportional to the incoming particle energy, E , and the energy resolution varies as $1/\sqrt{E}$. These features are present in compensating hadronic calorimeters. In this latter case, the energy resolution is worsened by the so-called *intrinsic fluctuations*, which take into account that a non negligible fraction of the incoming hadron energy is spent in breaking nuclear bounds, as for instance in nuclear spallation processes or in emitting largely undetected neutrons. In the calorimeter resolution, the extent of sampling fluctuations depends on both the type of passive absorbers and active media, as well as on the type of calorimetric structure realized, for instance thicknesses of passive absorbers. Active media commonly employed are scintillators, liquid argon, silicon detectors, gas detectors, etc.. Calorimeters with very a large volume (a few tens of m^3) have been constructed for high energy physics experiments. Specialized and compact electromagnetic calorimeters with imaging capabilities have been flown in balloon experiments. For all these systems, calibration procedures have been designed and set into operation in order to keep constantly calibrated and controlled many thousands of readout channels.

The very low interaction cross section between *Weakly Interacting Massive Particles*, WIMP, and the nuclei of the detector's active medium requires the use of very massive detectors to achieve a sensitivity level allowing the detection of WIMPs particles in the galactic environment. The effective cost of these detectors has to be minimized. Superheated droplet detectors, referred to as "bubble detectors" (see chapter on *Superheated Droplet (Bubble) Detectors*), of low cost, offer an attractive solution to the problem of WIMP detection. These detectors use superheated freon liquid droplets (active material) dispersed and trapped in a polymerized gel. This detection technique is based on the phase transition of superheated droplets at room or moderate temperatures. The phase transitions are induced by nuclear recoils when undergoing interactions with particles. These detectors are threshold detectors, a minimal energy deposition has to be achieved for inducing a phase transition. Their sensitivity to various types of radiation strongly depends on the operating temperature and pressure. Over the years, bubble detectors have been developed using detector formulations that are appropriate for a range of applications such as the direct measurement of neutralinos predicted by minimal supersymmetric models of cold dark matter, or portable neutron dosimeters for personal dosimetry or the measurement of the radiation fields in irradiation zones near particle accelerators or reactors.

Most of the instrumentations and experimental techniques developed for particle, nuclear and space physics have been used in medical applications. Furthermore, in this book, particular attention is paid to the physics mechanisms of radiation interaction with matter. These mechanisms, treated in the chapters on *Electromagnetic Interaction of Radiation in Matter* and on *Nuclear Interactions in Matter*, are of very important for the understanding of detectors and detector systems commonly used in nuclear medicine and in general for *medical applications*. In the chapter on *Medical Physics Applications*, imaging techniques based on *Magnetic Resonance Imaging (MRI)*, *Single Photon Emission Computed Tomography (SPECT)* and *Positron Electron Tomography (PET)* are treated. The main advantage of MRI is that no radioactive material is needed, i.e., it exploits the non-zero spin property of some nuclei. MRI uses magnetic fields varying from 0.2 to 2 T and radio frequency waves to observe the magnetization change of the non-zero spin nuclei. The isotope of hydrogen, ^1H , which has a nuclear spin of $\frac{1}{2}$, is a major component of the human body and is used as the main source of information. Both SPECT and PET make use of properties of photon interactions in matter. For SPECT, the gamma-ray imaging technique proceeds through the injection into the patient of a radioactive substance which emits photons of well-defined energy. The distribution of radionuclides, position and concentration, inside patient's body is monitored externally through the emitted radiation deposited in a photon detector array rotating around the body and which allows the acquisition of data from multiple angles. PET is a nuclear medical imaging technique which relies on the measurement of the distribution of a radioactive tracer or radiopharmaceutical labeled with a positron emitting

isotope injected into a patient. The positron emitted by the radioactive tracer or radiopharmaceutical annihilates very close to the emission point (≤ 1 mm) with an electron of the body to produce a pair of 511 keV photons emitted back-to-back, which in turn are detected by the PET camera.

It is important to note that many detectors rely partially or crucially on low-noise electronics. Most of the more visible and useful detector applications have been achieved through the usage of cheap monolithic electronics, designed and developed for fundamental physics researches and afterwards adjusted to other applications.

1.6.3 Radiation Environments and Silicon Devices

In the revised edition of this book, basic mechanisms resulting in temporary and/or permanent radiation-damages to silicon detectors and devices are presented and discussed for i) low- and high-resistivity bulk material and ii) in most cases up to cryogenic temperature. A review on permanent damage inflicted to silicon devices operated in radiation environments was provided by Leroy and Rancoita (2007).

Silicon is the active material of radiation detectors and in electronic devices used in the fabrication and development of electronic circuits of large to very large scale integration (VLSI) applications. As discussed in the previous section, these devices are commonly used for a large variety of applications in many fields including particle physics experiments, reactor physics, nuclear medicine, and space. These fields generally present adverse (or, even, very adverse) radiation environments that may affect the operation of the devices and are described in the chapter on *Radiation Environments and Radiation Damage in Silicon Semiconductor*. These environments are generated by i) the operation of the high-luminosity machines [e.g., the Large Hadron Collider[¶] (LHC)] for particles physics experiments, ii) the cosmic rays and trapped particles of various origins in interplanetary space and/or Earth magnetosphere and iii) the operation of nuclear reactors. Their potential threats to the devices operation, in terms of radiation-induced damage by displacement are also described in that chapter. Furthermore to understand the way it may affect the devices operation, the particles energy deposition mechanisms are discussed with i) the radiation-induced damage and ii) resulting effect on bulk and device parameters evolution. These latter modifications depend on the type of irradiation particles, their energy and irradiation fluence. A treatment is done of damage inflicted by total ionizing dose and non-ionization energy-loss (NIEL) effects for which the accumulated fluence causes permanent degradation because of the induced displacement damage.

In the case of irradiated detectors, the study of the peak evolution with bias voltage in spectroscopy measurement and irradiation fluence allows the measurement of the charge collection efficiency degradation (in various regions of the diodes) and structure alteration. The chapter on *Solid State Detectors* also includes a discussion

[¶]This machine is located at CERN (Geneva, Switzerland).

of the violation of non-ionizing energy-loss (NIEL) scaling. This *scaling property*, which expresses the proportionality between NIEL-value and resulting damage effects, is *violated* for low energy ($\lesssim 10$ MeV) protons.

Integrated radiation dose delivered by a high particle flux may permanently damage silicon detectors and electronics. This is a total dose effect which leads to degradation due to displacement damage and particle interaction and is reviewed in the chapter on *Displacement Damage and Particle Interactions in Silicon Devices*, where features (under large irradiations) of VLSI bipolar transistors are treated. These devices are mostly affected by the displacement damage generated by non-ionizing energy-loss processes. For instance, at large cumulative irradiation this mechanism was found to be responsible i) for the decrease of the gain of bipolar transistors mostly as a result of the decrease of the minority-carrier lifetime in the transistor base and ii) for the degradation of the series-noise performance of charge-sensitive-preamplifiers with bipolar junction transistors in the input stage, mainly because of the increase of the base spreading-resistance. The gain degradation depends almost linearly on the amount of the displacement damage generated (e.g., the amount of energy deposited by NIEL processes) independently of the type of incoming particle, thus following an approximate *NIEL-scaling*.

However, temporary or permanent damage may be inflicted by a single particle (*single event effect* - SEE) to electronic devices or integrated circuits. Chapter 7 contains also a large section on temporary and permanent damage inflicted by a single particle (single event effect) to electronic devices or integrated circuits. The generation of SEE in the various radiation field environments, and calculation of their rate of occurrence using data and simulation techniques are outlined. It is also emphasized that the understanding of radiation effects (not only SEE) on the silicon devices combined with simulation techniques has an impact on device design and allows the prediction of the behavior of specific devices, when exposed to a radiation field of interest. On several occasions, emphasis is put on the fact that the understanding of the principles of radiation effects on silicon devices combined with simulation techniques has an impact on device design and allows one to predict the behavior of specific devices in radiation environments.